Science Bulletin 67 (2022) 971–976

Contents lists available at ScienceDirect

Science Bulletin

journal homepage: www.elsevier.com/locate/scib

Article

Stabilization of S_3O_4 at high pressure: implications for the sulfur-excess paradox

HPSTAR 1411-2022

Siyu Liu [a,1], Pengyue Gao [a,1], Andreas Hermann [b], Guochun Yang [c], Jian Lü [a,*], Yanming Ma [a,d], Ho-Kwang Mao [e,*], Yanchao Wang [a,*]

[a] State Key Laboratory of Superhard Materials & International Center of Computational Method and Software, College of Physics, Jilin University, Changchun 130012, China
[b] Centre for Science at Extreme Conditions and Scottish Universities Physics Alliance, School of Physics and Astronomy, The University of Edinburgh, Edinburgh EH9 3FD, UK
[c] State Key Laboratory of Metastable Materials Science & Technology and Key Laboratory for Microstructural Material Physics of Hebei Province, School of Science, Yanshan University, Qinhuangdao 066004, China
[d] International Center of Future Science, Jilin University, Changchun 130012, China
[e] Center for High Pressure Science and Technology Advanced Research, Beijing 100094, China

ARTICLE INFO

Article history:
Received 28 July 2021
Received in revised form 19 December 2021
Accepted 20 December 2021
Available online 12 January 2022

Keywords:
Crystal structure prediction
High-pressure chemistry
S-bearing minerals
Sulfur cycle
Excess sulfur

ABSTRACT

The amount of sulfur in SO_2 discharged in volcanic eruptions exceeds that available for degassing from the erupted magma. This geological conundrum, known as the "sulfur excess", has been the subject of considerable interests but remains an open question. Here, in a systematic computational investigation of sulfur-oxygen compounds under pressure, a hitherto unknown S_3O_4 compound containing a mixture of sulfur oxidation states +II and +IV is predicted to be stable at pressures above 79 GPa. We speculate that S_3O_4 may be produced via redox reactions involving subducted S-bearing minerals (e.g., sulfates and sulfides) with iron and goethite under high-pressure conditions of the deep lower mantle, decomposing to SO_2 and S at shallow depths. S_3O_4 may thus be a key intermediate in promoting decomposition of sulfates to release SO_2, offering an alternative source of excess sulfur released during explosive eruptions. These findings provide a possible resolution of the "excess sulfur degassing" paradox and a viable mechanism for the exchange of S between Earth's surface and the lower mantle in the deep sulfur cycle.

1. Introduction

Sulfur (S) is one of the major multi-valent volatile elements distributed broadly throughout the Earth, participating in a variety of fundamental geochemical processes (e.g., global biochemical circulation [1], metal transport [2], atmospheric S loading during volcanic eruptions, and core–mantle segregation [3], etc.). The chemical speciation of S is strongly influenced by the wide range of oxidation states available. Under highly reducing environments, it dominantly exhibits an oxidation state of −II as sulfide, whereas under strongly oxidizing conditions, it has an oxidation state of +VI in sulfate. Other chemical species where S takes up intermediate oxidation states, such as polysulfides, elemental S, sulfite, or thiosulfate sulfite, may also exist in different geochemical settings [2,4,5]. The behavior of S in natural processes associated with complex oxidation–reduction reactions is unpredictable due to these variable oxidation states across the range of −II to +VI. Therefore, the geochemical behavior of S is thus replete with paradoxes, and there are many open questions concerning geochemical processes related to S-bearing minerals.

A well-known geological paradox, "sulfur excess degassing", has been recorded at numerous subduction zone volcanoes [6,7], where the amount of S (principally in the form of SO_2) released during explosive eruptions may be orders of magnitude higher than that estimated for degassing of the erupted melt [5]. Various sources for the excess S released by magmas in volcanic emissions [8,9] have been proposed, including dissolution in silicate liquid [10,11] or a coexisting gas phase at depth before eruption [7,12], gas expulsion from magma mixing [13,14], crystallization-induced exsolution (second boiling) [15], or the breakdown of S-bearing minerals [16], etc. These mechanisms are based on magmatic systems related to volcanic eruptions in shallow crust. However, the ultimate source of S found near the Earth's surface is derived from the Earth's mantle [17]. Oxygen, as one of the most abundant elements, provides critical control on the nature of Earth S reservoirs. Compounds formed by S and O have important implications for geochemical processes and the nature of these

* Corresponding authors.
E-mail addresses: lvjian@jlu.edu.cn (J. Lü), maohk@hpstar.ac.cn (H.-K. Mao), wyc@calypso.cn (Y. Wang).
[1] These authors contributed equally to this work.

https://doi.org/10.1016/j.scib.2022.01.005
2095-9273/

S reservoirs. Key questions that need to be resolved regards the formation and properties of S–O compounds under mantle conditions.

Various S–O compounds such as SO_2 [18], SO_3 [19,20], S_7O [21], and S_8O [22] have been proposed experimentally at ambient pressure. However, the high pressures characteristic of the mantle may strongly modify the chemical properties of elements and promote the formation of unexpected minerals [23–26]. Several high-pressure SO_3 phases have been proposed theoretically [27], but only SO_2 has been studied experimentally at pressures of up to 60 GPa [28], and S–O compounds are not well understood at high pressures. A pressing task is therefore to investigate the viability of S–O compounds under pressure conditions relevant to the Earth's mantle.

Here, we report an extensive exploration of high-pressure phase diagrams of S–O compounds. Besides known SO_2 and SO_3 compounds, an unexpected stoichiometry of S_3O_4 with an intriguing crystal structure, containing a mixture of +II and +IV S oxidation states, is predicted to appear at high pressures. We show that S_3O_4 is produced in reactions of sulfates and sulfides with iron and goethite under high pressure conditions in the deep mantle, decomposing to SO_2 and S under low *P-T* conditions at shallow depths of the Earth, thus offering insight into S cycles, and the origin of excess S degassing in volcanic eruptions.

2. Methods

Crystal structure searches on S_xO_y (x = 1–3, y = 1–4) at pressures of 50, 70, and 100 GPa were undertaken using the swarm intelligence based-CALYPSO method [29–31], which has successfully resolved crystal structures of many materials at high pressures [32]. Note that the maximum simulation cell for structure searches contains 40 atoms for each composition. Structural optimization, electronic structure, and phonon calculations were performed in a framework of density functional theory within the generalized gradient approximation [33] as implemented in the Vienna *ab initio* simulation package (VASP) [34]. Electron-ion interaction was described by projector augmented-wave potentials [35], with $3s^23p^4$ and $2s^22p^4$ configurations treated as the valence electrons of S and O, respectively. We also performed the full-potential all-electron calculations for the equation of state for SO_3 over the considered pressure range using the WIEN2k code [36]. VASP results were near identical to those of the all-electron calculations (Fig. S1 online), validating the accuracy of the pseudopotentials. A kinetic cut-off energy of 900 eV and a spacing of $2\pi \times 0.03$ Å^{-1} for Monkhorst-Pack *k*-mesh sampling [37] were adopted to give converged total energies (~1 meV/atom). Ionic positions were fully relaxed until the residual force acting on each ion was less than 1 meV/Å. Due to the layered structure of S_3O_4, the influence of van der Waals (vdW) interactions was considered using the optB88-vdW functional [38]. To describe the localized 3d electrons of Fe atoms in reactants, we considered electron correlation by using the GGA + U [39] method, with on-site Coulomb interaction of U = 5.0 eV and a Hund coupling constant of J = 0.8 eV [40]. The dynamic stabilities of the predicted new phase of S_3O_4 were verified by phonon calculations using the Hellmann-Feynman theorem with the finite displacement method of the 2 × 2 × 2 supercells containing 112 atoms, as implemented in the PHONOPY code [41,42].

3. Results

The main structure search results are depicted in convex hull diagrams in Fig. 1a. The energetic stabilities of various S–O structures were evaluated from their formation enthalpies relative to

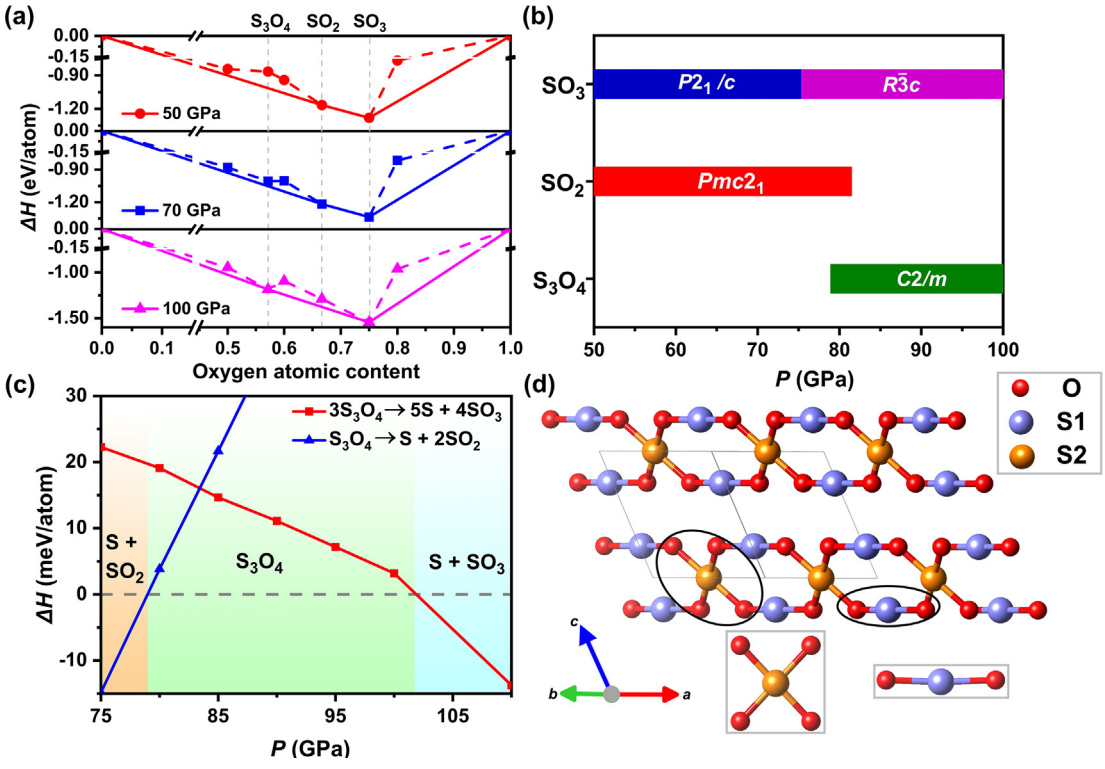

Fig. 1. Relative thermodynamic stability of the S–O system at 0 K. (a) Convex hull data of the $S_{1-x}O_x$ system at 50, 70, and 100 GPa. Formation enthalpies, ΔH, for each structure were calculated with respect to elemental S and O solids by $\Delta H(S_{1-x}O_x) = H(S_{1-x}O_x) - (1-x)H(\text{S solid}) - xH(\text{O solid})$ ($0 < x < 1$). Known S-III [43], S-IV [44], and ε-O_2 [45] phases were selected as the reference structures in the corresponding stable pressure ranges. Stable structures are located on the solid lines, and metastable structures sit on the dashed lines. (b) Predicted pressure-composition phase diagram of S–O phases. (c) Calculated pressure-enthalpy diagram for the reactions $3S_3O_4 \rightarrow 4SO_3 + 5S$ and $S_3O_4 \rightarrow 2SO_2 + S$ using optB88-vdW functional. The zero-point energy was included in the above energy calculations. (d) Crystal structure of *C*2/*m*-S_3O_4 containing mixed two-fold (S1) and four-fold (S2) coordination of S.

dissociation products of the relevant elemental S [43,44] and O solids [45]. At pressures of 50 and 70 GPa, the known stoichiometries SO_2 and SO_3 were readily identified as being stable in the structure search simulations. SO_3 was found to be the most stable phase against decomposition throughout the studied pressure range (50–100 GPa). At 100 GPa, an unexpected composition of S_3O_4 became stable with respect to the dissociation products of elemental S and SO_3 (Fig. S2 online). More detailed structural information can be found in Table S1 (online). Predicted stable pressure ranges for the considered structures are listed in Fig. 1b. S_3O_4 is energetically favorable relative to decomposition into elemental S and SO_2 or SO_3 in the pressure range of 79–102 GPa (Fig. 1c). The emergence of S_3O_4 leads to the instability of SO_2 above 81.5 GPa. The different exchange–correlation functionals and vdW methods have also demonstrated the stability of S_3O_4 at high pressure and temperature (*P-T*) (Figs. S3 and S4 online). We calculated phonon dispersions and observed no imaginary frequencies for the S_3O_4 structures at 100 GPa (Fig. S5 online), indicating that the predicted structure is dynamically stable.

The structure of S_3O_4 (Fig. 1d) is inherently layered and contains mixed two- and four-fold S coordination. Specifically, S1 is linearly coordinated to two O atoms, and S2 is square-coordinated to four O atoms. All S atoms are bonded to two adjacent S atoms, thus forming zigzag polymeric all-S chains. The S1–S1 and S1–S2 bond lengths are 2.22 and 2.13 Å at 80 GPa, respectively, slightly longer than the S–S bond lengths (2.01 Å) in the S-III phase, therefore indicating relatively weaker covalent S–S bonding. To further elucidate the nature of the bonding, we have examined the electron localization function (ELF) [46] of S_3O_4 in the (100) and (010) planes (Fig. 2a). Two inequivalent S atoms were clearly seen, with a less localized charge distribution is seen on the S–O bonds, indicating a significant degree of ionicity between the O anions and S cations. Clear covalent S–S bonding is indicated by the strong charge localization between the nearest neighbor S–S.

The oxidation states of S in geological environments play pivotal roles in planetary chemical and physical dynamics [49]. In general, the oxidation state of an element is closely related to local coordination and charge transfer. The S oxidation states in SO_2 and SO_3 can be assigned unambiguously as +IV and +VI, respectively. In contrast, the two- and four-fold coordination of S atoms with O atoms in S_3O_4 reveals its mixed-valence state. A Bader charge analysis [50], summarized in Table 1, supports this interpretation. The Bader charges systematically underestimate the formal charge state (O^{2-} here has a charge $-1.28e$ in the SO_2). In SO_3, S has a formal charge state of +VI, with a charge transfer of $3.90e$ from S to O, similar to that in SF_6 ($\sim 3.73e$). In SO_2, S has a formal charge state of +IV, with a charge transfer is $2.56e$. In S_3O_4, the partial charge of $2.68e$ in square-coordinated S2 almost equals that of the SO_2 case, so S2 can be considered as having an oxidation state of +IV. However, S1 is significantly less positively charged ($1.04e$) than the S^{+4} anion in SO_2. This highlights a crucial distinction of the S1 from S in SO_2, indicating that the linearly coordinated S1 in S_3O_4 adopts the rare +II S oxidation state.

Table 1
Partial charges for various S–O compounds obtained from Bader integration at 80 GPa.

Compounds	S (*e*)		O (*e*)
	S1	S2	
S_3O_4	+1.04	+2.68	−1.19
SO_2	+2.56		−1.28
SO_3	+3.90		−1.30

S–O compounds tend to be insulating, with satisfaction of the octet rule usually leading to the opening of a band gap. This rule is applicable to the predicted polymeric phases of SO_2 and SO_3. However, in S_3O_4, two bands were found to cross the Fermi level, forming an electron pocket around the *Z* point and a hole pocket spanning the *X* and *Y* points (Fig. 2b), giving rise to a clear metallic character of S_3O_4. The projected density of states (Fig. 2b) indicates that both O and linearly coordinated S1 contribute to the density of electronic states at the Fermi level, with the latter contribution being dominant. The metallic character originates from an overlap of the S1 electron lone pairs, which depends on the interlayer distance (Fig. S6 online).

Both S and O are typical light elements, so the stability of S–O compounds may be sensitive to temperature. To assess viability at high temperature, we further examined their energetic and structural stability under high *P-T* conditions. The free energies, including vibrational contributions and entropic effects, were evaluated for each phase using the quasi-harmonic approximation [51]. Formation enthalpy calculations further indicate that S_3O_4 is energetically favorable relative to decomposition into SO_3 and S above 70 GPa, with temperature having a minor effect on threshold pressure (Fig. 3a). Against decomposition into SO_2 and S, the stability region of S_3O_4 shifted to higher pressures with increasing temperature, from 79 GPa at 0 K to 100 GPa at 2300 K (Fig. 3b). *Ab-initio* molecular dynamics calculations indicate that S_3O_4 remains firmly solid at 2000 K at pressures of 80–100 GPa, corresponding to deep mantle conditions (Fig. S7 online), indicating that S_3O_4 may exist in solid form in the deep mantle. Overall, the predicted S_3O_4 is stable under *P-T* conditions relevant to the Earth's lower mantle [52], but decomposes into SO_2 and S at low pressure.

It is well known that the exchange of S between the Earth's surface and mantle, involving transport of S to the mantle via subduction and return to the surface by volcanic degassing, results in a global S cycle [53]. Nearly 43.6 Tg per year of S in the form of such as sulfates (e.g., $CaSO_4$ and $MgSO_4$ [53]) and sulfides (e.g., FeS and FeS_2 [54,55]) are subducted into the deep mantle [17]. However, the average annual SO_2 flux from erupting volcanoes is estimated to be 11.9 Tg (1 Tg = 10^{12} g) [56]. The cycle involves transformations

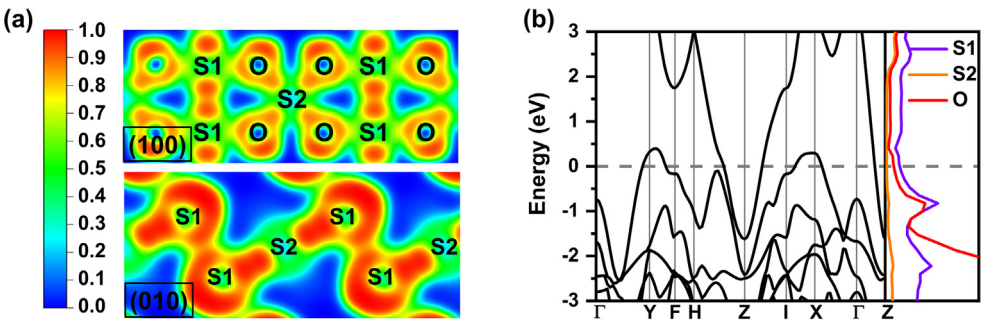

Fig. 2. The electronic properties of S_3O_4. (a) Calculated ELF in the (100) and (010) planes of *C2/m*-S_3O_4 at 80 GPa. (b) Band structures and projected density of states of *C2/m*-S_3O_4 at 80 GPa. Dashed line indicates the Fermi level. Band structures were calculated using the Heyd–Scuseria–Ernzerhof hybrid functional [47,48].

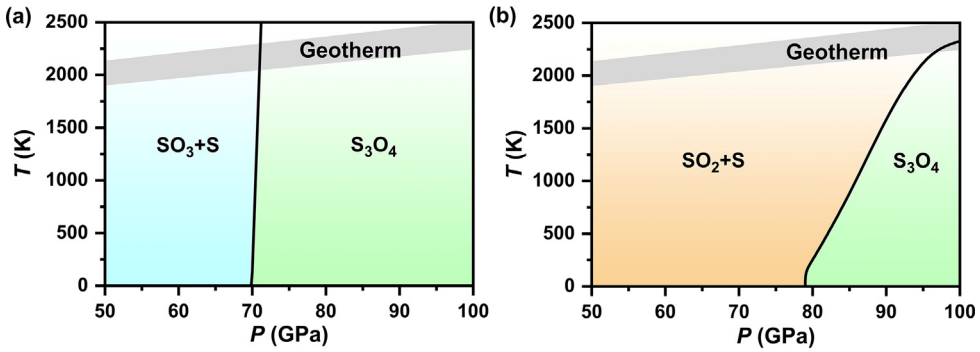

Fig. 3. The *P-T* phase diagrams for the reactions of $4SO_3 + 5S \rightarrow 3S_3O_4$ (a) and $2SO_2 + S \rightarrow S_3O_4$ (b). The geotherm curve was adapted from Ref. [52]

of S species via redox-driven chemical processes such as sulfate reduction and sulfide oxidation. It is estimated that ~1 wt% metallic Fe is present due to self-reduction reactions in the lower mantle [57]. In addition, the pyrite-type FeOOH may survive under the *P-T* conditions of the lower mantle within deeply subducted slabs [58]. Therefore, we explored the possibility of S_3O_4 production through decomposition of sulfates with Fe as a reducing agent or through oxidation reactions of sulfides with FeOOH as an oxidizing agent. We explored 39 possible reaction routes (Fig. 4a), in which iron oxides and hydrogen-bearing minerals that may exist in the

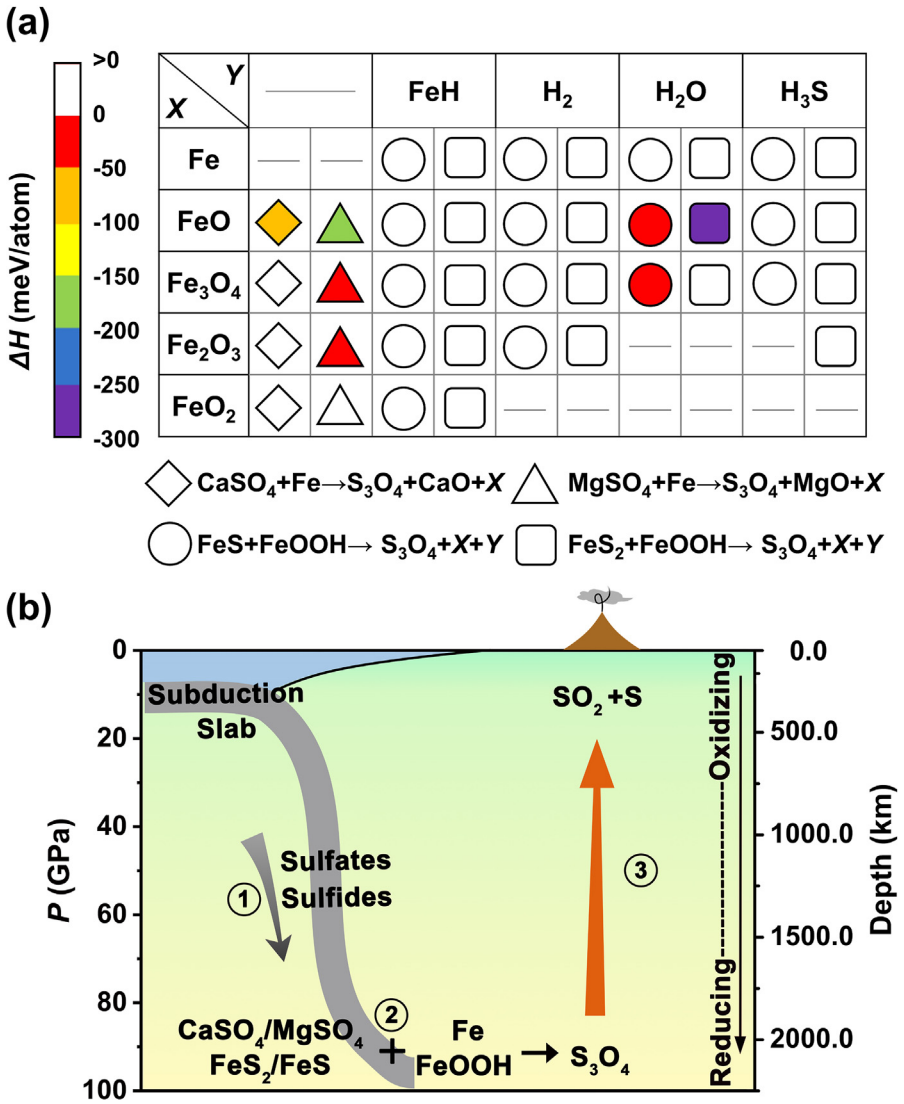

Fig. 4. Phase equilibria and the proposed S cycle in Earth. (a) Relative enthalpy of proposed reactions forming S_3O_4 at 100 GPa. Rhombus and triangle markers represent the reactions of $CaSO_4$ and $MgSO_4$ with iron; circles and squares represent the reactions of FeS and FeS_2 with FeOOH. *X* and *Y* represent different iron-oxides and hydrogen-bearing compounds, respectively. Colors denote enthalpies for the corresponding reactions. Crystal structures adopted to evaluate enthalpies are presented in Table S2 (online). (b) Processes proposed for the exchange of S between the Earth's surface and mantle: ① sulfates and sulfides are subducted into the deep mantle; ② subducted sulfates and sulfides react with the Fe or FeOOH to produce S_3O_4; and ③ S_3O_4 decomposes to SO_2 and elemental S, with emission of SO_2 to the surface via volcanism.

Earth's interior were chosen as products. The calculated negative reaction enthalpies of seven routes support the formation of S_3O_4 via redox reactions at 100 GPa, reflecting deep-mantle pressure. The pressure dependence of enthalpies of these reactions is shown in Fig. S8 (online). According to our calculations, S_3O_4 can be produced by two almost opposing mechanisms (i.e., reduction of sulfates and oxidation of sulfides), with these reactions being strongly dependent on redox conditions. It is well known that redox conditions have evolved continuously in the Earth's history [59]. Therefore, S_3O_4 compounds may have been produced by redox reactions involving S-bearing minerals throughout geological history.

Our results indicate three possible processes for S cycling in the Earth (Fig. 4b). Firstly, S-bearing sulfates or sulfides (e.g., $CaSO_4$, FeS_2 [60], and FeS [61]) are transported to the deep mantle in subduction slabs. They react with Fe or FeOOH (present in the mantle) to produce S_3O_4 under reducing or oxidizing conditions. If S_3O_4 formed in the deep mantle ascends (through mantle dynamic processes) to shallow depths of the Earth with low pressure conditions, it decomposes to S and SO_2, with the latter being the main form of S released during explosive eruptions (Fig. 3b). The mechanism of direct decomposition of S-bearing minerals (e.g., $CaSO_4$, FeS_2, and FeS) to release SO_2 as an explanation of the sulfur-excess paradox is not supported, even at high pressure [11] (see Fig. S9 online for enthalpy calculations); however, S_3O_4, which has not been considering previously, provides an alternative S reservoir in the deep mantle, completing the deep S cycle and aiding explanation of the paradox in volcanic eruptions, especially in some hotspots and for mantle plume volcanism (e.g., Nyamuragira volcano) [62].

4. Conclusion

A hitherto unknown compound, S_3O_4, has been identified as being stable under the high *P-T* conditions of the deep mantle. It contains a mixture of S(II) and S(IV) oxidation states and exhibits a peculiar metallic nature. A systematic examination of formation and decomposition reactions indicates that S_3O_4 may be a key factor in promoting redox reactions of sulfate or sulfide in the deep mantle and in the release of SO_2 at shallow depths, thereby offering insight into the origin of excess S degassing observed in volcanic eruptions. These results are of fundamental significance and have implications for processes in chemistry and geoscience; further experimental exploration is expected.

Conflict of interest

The authors declare that they have no conflict of interest.

Acknowledgments

This work was supported by the National Natural Science Foundation of China (12034009, 91961204, 11774127, 12174142, 11404128, 11822404, 52090024 and 11974134) and the Program for Science and Technology Innovative Research Team of Jilin University. Part of the calculation was performed in the high-performance computing center of Jilin University.

Author contributions

Yanchao Wang conceived and designed the project; Siyu Liu, Pengyue Gao, and Yanchao Wang performed simulations; Siyu Liu, Pengyue Gao, Andreas Hermann, Guochun Yang, Jian Lü, Yanming Ma, Ho-Kwang Mao, and Yanchao Wang performed data analysis and interpretation of the results; Siyu Liu, Pengyue Gao, Jian Lü, Yanming Ma, Ho-Kwang Mao, and Yanchao Wang wrote the paper; and all authors contributed to discussions of the results and revisions of the manuscript.

Appendix A. Supplementary materials

Supplementary materials to this article can be found online at https://doi.org/10.1016/j.scib.2022.01.005.

References

[1] Steudel R. Sulfur-rich oxides SnO and SnO_2 (n>1). In: Steudel R, editor. Elemental Sulfur und Sulfur-Rich Compounds II. Berlin: Springer; 2003. p. 203–30.
[2] Pokrovski GS, Dubrovinsky LS. The S^{3-} ion is stable in geological fluids at elevated temperatures and pressures. Science 2011;331:1052–4.
[3] Wang Z, Becker H. Ratios of S, Se and Te in the silicate Earth require a volatile-rich late veneer. Nature 2013;499:328–31.
[4] Barré G, Truche L, Bazarkina EF, et al. First evidence of the trisulfur radical ion S^{3-} and other sulfur polymers in natural fluid inclusions. Chem Geol 2017;462:1–14.
[5] Keppler H. Experimental evidence for the source of excess sulfur in explosive volcanic eruptions. Science 1999;284:1652–4.
[6] Wallace PJ, Gerlach TM. Magmatic vapor source for sulfur dioxide released during volcanic eruptions: evidence from Mount Pinatubo. Science 1994;265:497–9.
[7] Shinohara H. Excess degassing from volcanoes and its role on eruptive and intrusive activity. Rev Geophys 2008;46:RG4005.
[8] Wallace PJ, Edmonds M. The sulfur budget in magmas: evidence from melt inclusions, submarine glasses, and volcanic gas emissions. Rev Mineral Geochem 2011;73:215–46.
[9] Edmonds M, Woods AW. Exsolved volatiles in magma reservoirs. J Volcanol Geoth Res 2018;368:13–30.
[10] Keppler H. The distribution of sulfur between haplogranitic melts and aqueous fluids. Geochim Cosmochim Acta 2010;74:645–60.
[11] Masotta M, Keppler H, Chaudhari A. Fluid-melt partitioning of sulfur in differentiated arc magmas and the sulfur yield of explosive volcanic eruptions. Geochim Cosmochim Acta 2016;176:26–43.
[12] Lierenfeld MB, Zajacz Z, Bachmann O, et al. Sulfur diffusion in dacitic melt at various oxidation states: implications for volcanic degassing. Geochim Cosmochim Acta 2018;226:50–68.
[13] Edmonds M, Aiuppa A, Humphreys M, et al. Excess volatiles supplied by mingling of mafic magma at an andesite arc volcano. Geochem Geophys Geosyst 2010;11:Q04005.
[14] Kress V. Magma mixing as a source for Pinatubo sulphur. Nature 1997;389:591–3.
[15] Su Y, Huber C, Bachmann O, et al. The role of crystallization-driven exsolution on the sulfur mass balance in volcanic arc magmas. J Geophys Res-Solid Earth 2016;121:5624–40.
[16] Devine JD, Sigurdsson H, Davis AN, et al. Estimates of sulfur and chlorine yield to the atmosphere from volcanic eruptions and potential climatic effects. J Geophys Res-Solid Earth 1984;89:6309–25.
[17] Li J-L, Schwarzenbach EM, John T, et al. Uncovering and quantifying the subduction zone sulfur cycle from the slab perspective. Nat Commun 2020;11:514.
[18] Post B, Schwartz RS, Fankuchen I. The crystal structure of sulfur dioxide. Acta Crystallogr 1952;5:372–4.
[19] Westrik R, MacGillavry CH. The crystal structure of the asbestos-like form of sulphur trioxide. Acta Crystallogr 1954;7:764–7.
[20] Westrik R, Mac Gillavry CH. The crystal structure of the ice-like form of sulphur trioxide (γ-modification). Recl Des Trav Chim Des Pays-Bas 1941;60:794–810.
[21] Steudel R, Reinhardt R, Sandow T. Bond interaction in sulfur rings: crystal and molecular structure of cyclo-heptasulfur oxide, S_7O. Angew Chem Int Edit 1977;16:716.
[22] Luger P, Bradaczek H, Steudal R, et al. Röntgenstrukturanalyse von Cyclooctaschwefeloxid. Chem Ber 1976;109:180–4.
[23] Hu Q, Kim DY, Yang W, et al. FeO_2 and FeOOH under deep lower-mantle conditions and Earth's oxygen–hydrogen cycles. Nature 2016;534:241–4.
[24] Ji C, Li B, Liu W, et al. Crystallography of low Z material at ultrahigh pressure: case study on solid hydrogen. Matter Radiat Extrem 2020;5:038401.
[25] Mao HK, Chen B, Chen J, et al. Recent advances in high-pressure science and technology. Matter Radiat Extrem 2016;1:59–75.
[26] Li M, Liu T, Wang Y, et al. Pressure responses of halide perovskites with various compositions, dimensionalities, and morphologies. Matter Radiat Extrem 2020;5:018201.
[27] Tamm T, Pyykkö P. Possible high-pressure structures of sulfur trioxide. Chem Commun 2002;2:336–7.
[28] Zhang H, Tóth O, Liu X-D, et al. Pressure-induced amorphization and existence of molecular and polymeric amorphous forms in dense SO_2. Proc Natl Acad Sci USA 2020;117:8736–42.
[29] Wang Y, Lü J, Zhu L, et al. Crystal structure prediction via particle-swarm optimization. Phys Rev B 2010;82:094116.

[30] Wang Y, Lv J, Zhu L, et al. CALYPSO: a method for crystal structure prediction. Comput Phys Commun 2012;183:2063–70.
[31] Gao B, Gao P, Lu S, et al. Interface structure prediction via CALYPSO method. Sci Bull 2019;64:301–9.
[32] Wang Y, Ma Y. Perspective: crystal structure prediction at high pressures. J Chem Phys 2014;140:040901.
[33] Perdew JP, Burke K, Ernzerhof M. Generalized gradient approximation made simple. Phys Rev Lett 1996;77:3865–8.
[34] Kresse G, Furthmüller J. Efficient iterative schemes for *ab initio* total-energy calculations using a plane-wave basis set. Phys Rev B 1996;54:11169.
[35] Blöchl PE. Projector augmented-wave method. Phys Rev B 1994;50:17953–79.
[36] Blaha P, Schwarz K, Sorantin P, et al. Full-potential, linearized augmented plane wave programs for crystalline systems. Comput Phys Commun 1990;59:399–415.
[37] Monkhorst HJ, Pack JD. Special points for Brillouin-zone integrations. Phys Rev B 1976;13:5188–92.
[38] Klimeš J, Bowler DR, Michaelides A. Van der Waals density functionals applied to solids. Phys Rev B 2011;83.
[39] Dudarev SL, Botton GA, Savrasov SY, et al. Electron-energy-loss spectra and the structural stability of nickel oxide: an LSDA+U study. Phys Rev B 1998;57:1505–9.
[40] Jang BG, Kim DY, Shim JH. Metal-insulator transition and the role of electron correlation in FeO_2. Phys Rev B 2017;95:075144.
[41] Parlinski K, Li ZQ, Kawazoe Y. First-principles determination of the soft mode in cubic ZrO_2. Phys Rev Lett 1997;78:4063–6.
[42] Togo A, Oba F, Tanaka I. First-principles calculations of the ferroelastic transition between rutile-type and $CaCl_2$ type SiO_2 at high pressure. Phys Rev B 2008;78:134106.
[43] Degtyareva O, Gregoryanz E, Somayazulu M, et al. Novel chain structures in group VI elements. Nat Mater 2005;4:152–5.
[44] Hejny C, Lundegaard LF, Falconi S, et al. Incommensurate sulfur above 100 GPa. Phys Rev B 2005;71:020101.
[45] Fujihisa H, Akahama Y, Kawamura H, et al. O_8 cluster structure of the epsilon phase of solid oxygen. Phys Rev Lett 2006;97:085503.
[46] Savin A, Nesper R, Wengert S, et al. ELF: the electron localization function. Angew Chem Int Edit 1997;36:1808–32.
[47] Heyd J, Scuseria GE, Ernzerhof M. Hybrid functionals based on a screened Coulomb potential. J Chem Phys 2003;118:8207–15.
[48] Paier J, Marsman M, Hummer K, et al. Screened hybrid density functionals applied to solids. J Chem Phys 2006;124:154709.
[49] Stagno V, Ojwang DO, McCammon CA, et al. The oxidation state of the mantle and the extraction of carbon from Earth's interior. Nature 2013;493:84–8.
[50] Bader RFW. A quantum theory of molecular structure and its applications. Chem Rev 1991;91:893–928.
[51] Pavone P, Karch K, Schütt O, et al. *Ab initio* lattice dynamics of diamond. Phys Rev B 1993;48:3156–63.
[52] Nomura R, Hirose K, Uesugi K, et al. Low core-mantle boundary temperature inferred from the solidus of pyrolite. Science 2014;343:522–5.
[53] Jégo S, Dasgupta R. The fate of sulfur during fluid-present melting of subducting basaltic crust at variable oxygen fugacity. J Petrol 2014;55:1019–50.
[54] Smith EM, Shirey SB, Richardson SH, et al. Blue boron-bearing diamonds from Earth's lower mantle. Nature 2018;560:84–7.
[55] Smith EM, Shirey SB, Nestola F, et al. Large gem diamonds from metallic liquid in Earth's deep mantle. Science 2016;354:1403–5.
[56] Stoiber RE, Williams SN, Huebert B. Annual contribution of sulfur dioxide to the atmosphere by volcanoes. J Volcanol Geoth Res 1987;33:1–8.
[57] Frost DJ, Liebske C, Langenhorst F, et al. Experimental evidence for the existence of iron-rich metal in the Earth's lower mantle. Nature 2004;428:409–12.
[58] Nishi M, Kuwayama Y, Tsuchiya J, et al. The pyrite-type high-pressure form of FeOOH. Nature 2017;547:205–8.
[59] Frost DJ, McCammon CA. The redox state of Earth's mantle. Annu Rev Earth Planet Sci 2008;36:389–420.
[60] Bataleva YV, Palyanov YN, Borzdov YM, et al. Sulfidation of silicate mantle by reduced S-bearing metasomatic fluids and melts. Geology 2016;44:271–4.
[61] Prouteau G, Scaillet B. Experimental constraints on sulphur behaviour in subduction zones: implications for TTG and adakite production and the global sulphur cycle since the Archean. J Petrol 2013;54:183–213.
[62] Head EM, Shaw AM, Wallace PJ, et al. Insight into volatile behavior at Nyamuragira volcano (D.R. Congo, Africa) through olivine-hosted melt inclusions. Geochem Geophys Geosyst 2011;12:Q0AB11.

Siyu Liu is a Ph.D. candidate at State Key Laboratory of Superhard Materials & International Center of Computational Method and Software, College of Physics, Jilin University. Her current research mainly focuses on crystal structure prediction and high-pressure chemistry.

Jian Lü is an associate professor at State Key Laboratory of Superhard Materials & International Center of Computational Method and Software, College of Physics, Jilin University. After completing his Ph.D. degree in condensed matter physics from Jilin University in 2013, he then moved to Beijing Computational Science Research Center (China) for postdoctoral research. His research focuses on developments and applications of the CALYPSO structure prediction method for material discovery in fields of physics, chemistry, and materials science.

Yanchao Wang is a professor at State Key Laboratory of Superhard Materials & International Center of Computational Method and Software, College of Physics, Jilin University. He received his Ph.D. degree from Jilin University in 2013. After graduation, he joined the State Key Laboratory of Superhard Materials of Jilin University. His research interest mainly focuses on developing the structure prediction method and *ab initio* method based on orbital free density functional theory.

Ho-Kwang Mao is the Director of Center for High Pressure Science and Technology Advanced Research. He received his Ph.D. degree in 1968 from University of Rochester, and worked until 2018 at Geophysical Laboratory, Carnegie Institution of Washington on high-pressure research. He is a Member of National Academy of Sciences (USA), Member of Academia Sinica, Foreign Member of Chinese Academy of Sciences and Foreign Member of Royal Society of London. His research interest mainly focuses on deep Earth geophysics, pioneering high pressure technology, high pressure condensed-matter physics, high pressure chemistry, high pressure crystallography, and high-pressure materials science.